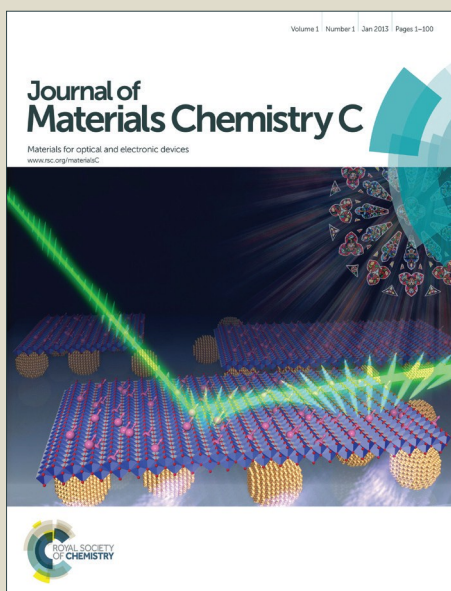


Journal of Materials Chemistry C

Accepted Manuscript



This is an *Accepted Manuscript*, which has been through the Royal Society of Chemistry peer review process and has been accepted for publication.

Accepted Manuscripts are published online shortly after acceptance, before technical editing, formatting and proof reading. Using this free service, authors can make their results available to the community, in citable form, before we publish the edited article. We will replace this *Accepted Manuscript* with the edited and formatted *Advance Article* as soon as it is available.

You can find more information about *Accepted Manuscripts* in the [Information for Authors](#).

Please note that technical editing may introduce minor changes to the text and/or graphics, which may alter content. The journal's standard [Terms & Conditions](#) and the [Ethical guidelines](#) still apply. In no event shall the Royal Society of Chemistry be held responsible for any errors or omissions in this *Accepted Manuscript* or any consequences arising from the use of any information it contains.

Thermoelectric Properties of Materials with Nontrivial Electronic Topology

Koushik Pal, Shashwat Anand, and Umesh V. Waghmare*

*Chemistry and Physics of Materials Unit and and
Theoretical Sciences Unit, Jawaharlal Nehru Centre for
Advanced Scientific Research, Bangalore 560064, India*

Abstract

Materials with good thermoelectric (TE) properties such as Bi_2Te_3 and SnTe have recently come to be known as topological insulators (TIs). It is fundamentally interesting to explore if other materials with non-trivial electronic topology may also exhibit good TE properties. In this work, we use first-principles density functional theoretical calculations to determine and analyze electronic thermoelectric properties (Seebeck coefficient (S), electrical conductivity (σ) and thermoelectric power factor(P)) of topological insulators ($\beta\text{-As}_2\text{Te}_3$, BiTeCl , PbTe), topological Dirac semimetal (Na_3Bi) and Weyl semimetal (TaAs) and semimetallic YPtBi , belonging to different symmetry and topological classes. We find that the multiple sub-band structure, small band gap of topologically insulators, and their vicinity to a metallic state associated with an electronic topological transition (ETT) are responsible for their superior TE performance. In addition, sensitivity of their electronic structure to strain makes their thermoelectric properties highly tunable. We predict that TaAs is a promising TE for experimental exploration, and propose that the thermoelectric modulators based on TIs such as SnTe and PbTe will be more efficient under mechanical load.

* Electronic mail:waghmare@jncasr.ac.in

I. INTRODUCTION

In recent years, thermoelectric (TE) materials have been a subject of significant research activity [1, 2], as they convert wasted energy in the form of heat into electricity, and provide an environment friendly all-solid state alternative to cooling technologies like refrigeration [4–6]. Thermoelectric power generators have also been used for long in space missions [7]. The Seebeck coefficient (S), a measure of the thermoelectric property, relates an electrical potential difference created from a temperature gradient in a TE material. Materials with large S can be versatile and robust for waste-heat recovery from various scenarios such as automobile exhaust systems, industrial furnaces, gas pipes etc. Recently, efficient conversion of solar energy to electrical energy has also been demonstrated using thermoelectric Seebeck effect [2].

The thermoelectric figure of merit (ZT) is defined as, $ZT = \sigma S^2 T / \kappa = PT / \kappa$, where σ is the electrical conductivity, κ is the thermal conductivity and $P (= \sigma S^2)$ is the thermoelectric power factor. Unlike many other important functionalities like piezoelectricity, ferroelectricity or multiferroicity, thermoelectricity is not restricted by any symmetry of a material. However, materials with efficient thermoelectric conversion ability are hard to engineer due to conflicting requirements like low thermal conductivity (κ) and high electrical conductivity (σ), and also competing factors such as carrier concentration and effective mass, which are evident in the simple expressions of S and σ , valid for metals and degenerate semiconductors [1],

$$S = \frac{8\pi^2 k_B^2 T}{3eh^2} m^* \left(\frac{\pi}{3n} \right)^{\frac{2}{3}}, \quad (1)$$

and

$$\sigma = \frac{ne^2\tau}{m_b^*}, \quad (2)$$

where k_B, T, n, τ are Boltzmann constant, temperature, carrier concentration and relaxation time respectively. m^* is the density-of-states effective mass given by $m^* = N_v^{2/3} m_b^*$, where m_b^* is the average band effective mass of a single valley given by $m_b^* = (m_x m_y m_z)^{1/3}$ and N_v is the valley degeneracy [3]. m_x, m_y and m_z are components of the effective mass tensor along three principle directions for an anisotropic material. While both S and σ occur in the numerator of the expression for ZT , they show opposite trends with effective mass and carrier concentration. Moreover, in metal the electronic contribution to thermal

conductivity (κ_{el}) is also linked to σ via the Wiedemann-Franz law [8] and effective mass of the charge carriers.

The dependences of S and σ on the density of states (DOS) at Fermi energy (E_F) are also, to a certain extent, conflicting. The dependence of S on local DOS at the Fermi level is captured by the Mott expression which, in general, holds for metals [9], but it is also applicable for semiconductors for which the Fermi level lies within a narrow region inside the density of states, where it increases locally [10].

$$\begin{aligned} S &= -\frac{\pi^2 k_B^2 T}{3e} \left\{ \frac{d[\ln(\sigma(\varepsilon))]}{d\varepsilon} \right\}_{\varepsilon=E_F} \\ &= -\frac{\pi^2 k_B^2 T}{3e} \left\{ \frac{1}{n} \frac{dn(\varepsilon)}{d\varepsilon} + \frac{1}{\mu(\varepsilon)} \frac{d\mu(\varepsilon)}{d\varepsilon} \right\}_{\varepsilon=E_F}, \end{aligned} \quad (3)$$

where energy dependent conductivity $\sigma(\varepsilon)$, which is generally known as the transport distribution function (see Eq. [7] for a more general definition) is given by,

$$\sigma(\varepsilon) = D(\varepsilon) f_0(\varepsilon) e \mu(\varepsilon) = n(\varepsilon) e \mu(\varepsilon), \quad (4)$$

where $D(\varepsilon)$, $f_0(\varepsilon)$, $\mu(\varepsilon)$ denote energy dependent DOS, Fermi-Dirac distribution function and charge carrier mobility respectively, and $n(\varepsilon) = D(\varepsilon) f_0(\varepsilon)$ denotes the carrier concentration. From Eq. [3], we see that a large S can be achieved by increasing $[\frac{dn(\varepsilon)}{d\varepsilon}]$, which in turn is caused by a local enhancement of $D(\varepsilon)$ [11].

Recently, materials with good thermoelectric properties, such as Bi_2Te_3 and PbTe , have been discovered also to exhibit non-trivial electronic topology at ambient [12, 13] and/or applied pressures [14]. Materials with nontrivial electronic topology are novel quantum states of matter which exhibit exotic and robust conducting surface states as a consequence of nontrivial topology of the electronic structure in their bulk form. It appears that materials exhibiting a non-trivial electronic topology or high thermoelectric figure of merit often comprise of heavy elements and possess small band gaps [15]. Heavy atoms have low frequencies of vibration that result in low lattice thermal conductivity essential for a high thermoelectric figure of merit. They also exhibit large spin orbit coupling necessary for certain nontrivial topological materials. In addition, topological insulators (TIs) often have a small electronic band gap as they lie in the vicinity of a strain dependent electronic topological transition

(ETT). This helps in tuning the intrinsic carrier concentration to optimize the thermoelectric power factor. ETT in a material involves a transformation from a topologically trivial to topologically nontrivial phase. It involves change in the overall topology of the occupied bands of a material characterized by topological invariants like Z_2 indices or Chern number.

Other features of electronic dispersion of a topologically non-trivial material may also be used favorably to enhance thermoelectric efficiency [16–20]. For example electronic structure of SnTe, which is a topological crystalline insulator (TCI), exhibits a heavy hole band near its light hole valence band maximum (VBM). Energy of the light and heavy hole bands can be brought closer (a phenomenon known as band convergence [3]) through alloying [18, 19], to optimize carrier mobility and enhance thermopower (S). Furthermore, ZT of TIs is strongly size dependent [20], taking values greater than 1 in nanoscale regime where the metallic surface states become more relevant to electric conduction. Clearly, the electronic structure of topologically nontrivial materials seems to have a great potential for efficient thermoelectric transport, and they may possess a high P even in the semi-metallic or small band gap regime. Here, we focus on determination of P of materials belonging to different classes of nontrivial topology, and uncover the correlation between the two.

We use semi-classical Boltzmann transport theory within a constant scattering time approximation to calculate the transport properties S , σ and P . As E_F is tunable by doping, we calculate S , σ and P of the compounds over a wide energy window (~ 1.6 eV) straddling the undoped E_F . Our calculations suggest that a high ZT in typical TE materials such as Bi_2Te_3 does not arise just from the strongly dispersing valence band (VB) and conduction band (CB) edges associated with the TI phase, but similar to ordinary band insulators (BIs), the TE properties of TIs too depend strongly on their density of states close (typically within ~ 0.5 eV) to the Fermi level. Due to vicinity to an ETT induced by strain, the TE properties of TIs (or corresponding BIs) are quite sensitive to strain. We demonstrate this for $\beta\text{-As}_2\text{Te}_3$, where applied strain not only closes the band gap but also aides in the band convergence to increase P by as a factor of 3. Our calculations reveal that PbTe exhibits better TE performance in its TCI phase than its BI phase. Contrary to naive expectation, our calculations also indicate that n-doped TaAs could be a promising thermoelectric with a high power factor.

This paper is organized as follows. In section II, we give a brief introduction to materials with different topologically nontrivial features, chosen in this work. In section III, we pro-

vide computational details which include (a) the method used in determination of electronic structure using first-principles calculations (section III A), and (b) a technique used to estimate electronic transport properties based on the semi-classical Boltzmann theory (section III B). We present our results in section IV and discuss them in section V, followed by a conclusion in section VI.

II. MATERIALS WITH NONTRIVIAL ELECTRONIC TOPOLOGY

Nontrivial electronic topology of a material often arises from the spin-orbit coupling (SOC) that is strong relative to crystal field splitting (e.g. Z_2 topological insulator [13]), which results in reordering or interchange of valence and conduction bands of distinct symmetries in a phenomenon known as band inversion. Certain crystallographic symmetries give rise to nontrivial topological phases in which symmetry protected linearly dispersing valence and conduction bands cross in the electronic structure of a bulk material (e.g. Dirac semimetal [21, 22], Weyl semimetal [23]), and gapless conducting states appear on its surface [24]. Depending on the dispersion of electronic bands near the Fermi level or gap of the bulk, surface states and their origin, we consider here six categories of topologically nontrivial materials: (a) Z_2 TI (centrosymmetric), (b) Z_2 TI (non-centrosymmetric), (c) TCI, (d) topological semimetal, (e) Dirac semimetal and (f) Weyl semimetal, and identify the correlation between their electronic topology and thermoelectric performance, if any.

A Z_2 TI exhibits a non-zero band gap in its bulk electronic structure, and gapless surface states with linearly dispersing bands forming a Dirac cone (or in odd numbers) that typically falls in the bulk band gap, which are protected by time reversal symmetry. In the TCI class of materials, crystal symmetry and field play more significant role than time reversal symmetry and SOC [24]. For example, SnTe (a TCI) has a mirror symmetry in its crystal structure [25], due to which it exhibits even number of band inversions (as a function of strain or pressure which modifies the relative strength of hybridization and crystal field splitting) in the electronic structure of its bulk. The robust surface states in this class of materials are protected by the mirror symmetry. In topological semimetals, VBM and CBM touch each other to give a semimetallic state, and the dispersion of bands is often quadratic at the touching point. In this class, the electronic structure possesses an inverted band order (as in HgTe) of the VBM and CBM compared to their band insulator counterpart (as in

CdTe) [26]. Materials with C_3 , C_4 or C_6 uniaxial rotational symmetries can host Dirac semimetallic states [27]. In a Dirac semimetal, a pair of doubly degenerate and linearly dispersing bands of different symmetries cross each other giving rise to a robust Dirac cone in their bulk electronic structure. In materials with broken spatial inversion or time reversal symmetries, the doubly degenerate bands split and become two non degenerate bands due to SOC. Despite these broken symmetries, if the non-degenerate bands make robust linear crossing, the material is a Weyl semimetal in which the point of crossing is doubly degenerate and is called a Weyl node.

We choose six materials belonging to six different categories as mentioned earlier and summarize their structural features in Fig. 1. Amongst the materials studied here, β -As₂Te₃ has a rhombohedral crystal structure with space group $R\bar{3}m$ (No. 166), which becomes a Z_2 TI as a function of uniaxial stress ($\sigma_{zz} > 1.77$ GPa) [28]. PbTe, which has a rocksalt structure with space group $Fm\bar{3}m$ (No. 225) undergoes electronic topologically transition with hydrostatic pressure (P) and becomes a TCI (for $P > 4$ GPa) [14]. Na₃Bi, with space group $P6_3/mmc$ (No. 194), is a Dirac semimetal in its native state [22], BiTeCl with space group $P6_3mc$ (No. 186) is a large band gap non-centrosymmetric Z_2 TI [29], and YPtBi in Half-Heusler structure with space group $F\bar{4}3m$ (No. 216) is a topological semimetal with vanishing gap [30]. Non centrosymmetric TaAs crystal with space group $I4_1md$ (No. 109) is a Weyl semimetal [23] at ambient pressure. Amongst these compounds, to the best of our knowledge, thermoelectric properties of only β -As₂Te₃ and PbTe have been investigated [3, 10, 31], albeit in their ambient pressure band insulating phases. Here, We determine the transport properties of β -As₂Te₃ and PbTe in both the BI and TI phases and other compounds in their topologically nontrivial phases. The thermoelectric performance of the electronically nontrivial topological phases of β -As₂Te₃, PbTe, BiTeCl, YPtBi, Na₃Bi and TaAs is assessed by comparing their power factors with that of band insulating PbTe which is an established high ZT TE.

III. COMPUTATIONAL METHODS

A. First-principles Density Functional Theory Calculations

We employ a full potential linearized augmented plane wave (FPLAPW) based method as implemented in the WIEN2k code [32] to determine the electronic structure and properties of all the materials presented here. To obtain the total energy and eigenvalues of the electrons in a solid using FPLAPW method, we use a basis set achieved by dividing the unit cell into non overlapping spheres centered around each atom and the interstitial regions. Plane wave basis set is used to represent wave functions inside the interstitial region, which is augmented by the atomic-like wave function inside the spherical region around each atom. We use Perdew, Burke and Ernzerhof parametrization [33] of the exchange correlation energy functional derived within a gradient generalized approximation [34]. Truncation of the plane wave expansion of electronic wave functions inside the interstitial region is specified by $R_{mt} * K_{max}$, where R_{mt} is the radius of the smallest atomic sphere (muffin-tin), K_{max} is the plane wave cut-off vector. Charge density cut-off is specified by G_{max} . The cut-off values for the wave functions and charge density are summarized in Table I. In all the calculations, we have included spin-orbit coupling through the second variational procedure [35, 36], and electronic structure (see Fig. 2) of the each of the materials is determined at the lattice constants (see Table I) by including the SOC in the Kohn-Sham Hamiltonian.

TABLE I. Structural parameters and cutoffs defining basis sets used in WIEN2k density functional theory (DFT) calculations of six materials that exhibit electronic structure with nontrivial topology. We use experimental lattice constants of all the compounds except for β -As₂Te₃ and PbTe which are trivial insulators at ambient pressure (marked with * in the table). We use lattice constants of β -As₂Te₃ and PbTe obtained with uniaxial strain $\epsilon_{zz} = -0.07$ [37] and isotropic strain (ϵ_h) = -0.01 [38] respectively. E_g is the smallest band gap, values of R_{mt} , K_{max} and G_{max} are used in defining the basis sets, and N_I is the number of inequivalent k-points in irreducible wedge of the Brillouin zone (IBZ) of each of the materials when the full Brillouin zone is sampled with 40,000 k-points.

Material	Lattice constants (\AA)	E_g (eV)	R_{mt} (a.u.)	K_{max} (a.u. ⁻¹)	G_{max} (Ry ^{1/2})	N_I
β -As ₂ Te ₃	a=4.089 c=28.184*	0	2.5 for As & Te	2.8 for As & Te	12.0	1563
PbTe	a=6.374*	0.10	2.0 for Pb & Te	3.5 for Pb & Te	12.0	1059
Na ₃ Bi	a=5.459, c= 9.675	0	2.0 for Na & Bi	3.5 for Na & Bi	12.0	1936
BiTeCl	a=4.2426, c= 12.397	0.48	2.5 for Bi, Te, & Cl	2.8 for Bi, Te, & Cl	12.0	1944
YPtBi	a=6.64	0	2.5 for Y, Pt, & Bi	2.8 for Y, Pt, & Bi	12.0	1059
TaAs	a=3.437, c=11.646	0.032	2.48 for Ta 2.36 for As	2.82 for Ta 2.97 for As	12.0	2835

B. Semi-classical Boltzmann Transport Theory

We use the density functional theory (DFT)-based electronic structure within a semi-classical Boltzmann theory under a constant scattering time approximation as implemented in the BOLTZTRAP code [39], and calculate electrical conductivity, Seebeck coefficient and power factor of the six materials described earlier (also see Fig. 1) as a function of Fermi

energy (E_F) and temperature (T). Electrical conductivity ($\sigma_{\alpha\beta}$) and Seebeck coefficient ($S_{\alpha\beta}$) which are tensor quantities are obtained using [11, 40]

$$\sigma_{\alpha\beta}(T, E_F) = \frac{1}{\Omega} \int \Sigma_{\alpha\beta}(\varepsilon) \left[-\frac{\partial f_0(T, \varepsilon, E_F)}{\partial \varepsilon} \right] d\varepsilon \quad (5)$$

and

$$S_{\alpha\beta}(T, E_F) = \frac{1}{eT\sigma_{\alpha\beta}(T, E_F)} \int (\varepsilon - E_F) \Sigma_{\alpha\beta}(\varepsilon) \left[-\frac{\partial f_0(T, \varepsilon, E_F)}{\partial \varepsilon} \right] d\varepsilon, \quad (6)$$

where α, β are Cartesian indices, Ω, f_0 are volume of unit cell, and Fermi-Dirac distribution function of the carriers respectively. Central to these relations is the transport distribution function ($\Sigma_{\alpha\beta}$),

$$\Sigma_{\alpha\beta}(\varepsilon) = \frac{e^2}{N} \sum_{i, \mathbf{k}} \tau v_{\alpha}(i, \mathbf{k}) v_{\beta}(i, \mathbf{k}) \delta(\varepsilon - \varepsilon_{i, \mathbf{k}}), \quad (7)$$

where \mathbf{k} and i are wave vector and band index, and N is the total number of \mathbf{k} -points used in sampling the Brillouin zone, τ is the relaxation time, and $v_{\alpha}(i, \mathbf{k}) = \frac{1}{\hbar} \frac{\partial \varepsilon_{i, \mathbf{k}}}{\partial \mathbf{k}_{\alpha}}$ is the group velocity. The derivative of the energy $\varepsilon_{i, \mathbf{k}}$ is determined by BOLTZTRAP code through Fourier expansion of band energies ($\bar{\varepsilon}_{i, \mathbf{k}}$) using the star functions of the space group symmetry [39]: $\bar{\varepsilon}_i(\mathbf{k}) = \sum_{\mathbf{R}} c_{\mathbf{R}i} S_{\mathbf{R}}(\mathbf{k})$ and $S_{\mathbf{R}}(\mathbf{k}) = \frac{1}{n} \sum_{\{\wedge\}} e^{i\mathbf{k} \cdot \wedge \mathbf{R}}$, where \mathbf{R} is a direct lattice vector, $\{\wedge\}$ are the n point group symmetry operations, and $c_{\mathbf{R}i}$ are the expansion coefficients. The point group symmetries and space group of each of the six materials are summarized in Fig. 1.

Band energies are determined on a dense mesh (40,000) of \mathbf{k} -points for sampling the Brillouin zone for each of the materials. The actual calculation uses the symmetry and \mathbf{k} -points only in the irreducible wedge of the corresponding Brillouin zone (see last column of Table I). To achieve better fit between $\bar{\varepsilon}_i(\mathbf{k})$ and $\varepsilon_{i, \mathbf{k}}$, the original grid of \mathbf{k} -points was interpolated onto a \mathbf{k} -mesh five times as dense. We calculate the transport properties using strained lattice constants [37, 38] for β -As₂Te₃, PbTe (at which they become TI and TCI respectively) and experimental lattice constants for Na₃Bi, BiTeCl, YPtBi, TaAs (see Table I). The limits of the integration in evaluation of σ and S (see Eq. [5] and Eq. [6]) span an interval $E_F - 0.5$ Ry to $E_F + 0.5$ Ry. As the relaxation time (τ) is an undetermined quantity in our simulations, quantities which depend on the τ (electrical conductivity and power factor) are reported by scaling them with τ (i.e. σ/τ and $S^2\sigma/\tau$).

IV. RESULTS

We determined transport properties namely σ/τ , S , and P (see Fig. 2) within a rigid band approximation (RBA) in which the electronic structure is assumed to be unchanged with doping. This approximation is reasonably good for low doping concentrations and is commonly used for theoretical study of TE materials [39–44]. Materials with good thermoelectric properties typically require one type (p or n-type) of majority carriers. Comparable concentrations of p and n-type carriers in a material lead to bipolar effects, and cause low ZT at high temperatures. Hence, semiconductors are typically doped to optimize carrier concentration and maximize thermoelectric efficiency [1]. Effects of doping concentration are thus determined essentially through the corresponding changes in the Fermi energy. To this end, we show the dependence of density of states (DOS) on energy and of S , σ/τ , $S^2\sigma/\tau$ on Fermi level (E_F), keeping E_F of the undoped compounds fixed at 0 eV. A positive E_F signifies n-type doping, while a negative E_F means p-type doping. The type of doping is also reflected in the sign of the Seebeck coefficient (S). Generally, S peaks at small doping levels and approaches values close to zero at large concentrations. Electrical conductivity (σ/τ) depends directly on the DOS, thus behavior of $\sigma(E_F)$ and DOS ($D(\varepsilon)$) are very similar.

The TE power factor $P(= S^2\sigma/\tau)$ is noticeably large and exhibits multiple peaks in the energy window chosen. We classify these peaks into three categories (type-I, type-II and type-III) based on their origin and assess their relevance to applications by their proximity to the undoped Fermi level (see Table II). The type-I peak occurs for doping concentrations where $D(\varepsilon)$ (and correspondingly $\sigma(\varepsilon)$) is large (see Eq. [3]). The maximum of the peaks in the power factor of the materials studied here is invariably (except for strained [38] PbTe) in the type-I peak. In most cases, the type-II peak in P occurs in the vicinity of the peak in S which is caused by a sharp energy dependence of $D(\varepsilon)$ (i.e. large $\frac{\partial D(\varepsilon)}{\partial \varepsilon}$), and occurs close to the undoped E_F (for example in YPtBi). Though these peaks are smaller in magnitude, they are more relevant to applications as they correspond to modest doping. The type-III peak in P as a function of Fermi energy appears when maxima in both $[\frac{\partial D(\varepsilon)}{\partial \varepsilon}]$ as well as S are close to each other, and arise as a convolution of type-I and type-II peaks. In the constant scattering time approximation, electronic conductivity increases with temperature (as the effects of temperature dependent scattering with time are neglected). Thus, it follows from Eq.[1], Eq.[3], and Eq.[6] that, P , σ/τ and S of topological nontrivial materials (either

with a finite gap or a vanishing gap) show similar behavior to that of a semiconductor with temperature, though the required doping levels for maximal P depend only slightly on temperature. We now discuss the transport properties of each of the six compounds in detail. Here, we determine the direct implications of electronic structure of these materials to their thermoelectric power rather comparing their thermoelectric performance, as the relaxation time (τ) varies from one material to another.

TABLE II. This table summarizes different types of peaks which appear in the power factor (P) of the materials with their positions along the Fermi level (E_{peak}) marked with Roman numerals I, II, and III for type-I, type-II and type-III peaks respectively. Negative and positive values of the E_{peak} mean n and p-type doping. Local maximum in power factor (P_{max}) is given for each of the materials at 300 Kelvin in the unit of $10^{14} \mu W cm^{-1} K^{-2} s^{-1}$.

Material	Type of doping	Type of peak	E_{peak} (eV)	P_{max} at 300 K
β -As ₂ Te ₃	p	I	-0.44	57
		II	-0.2	48
	n	I	0.54	53
		II	0.17	35
PbTe	p	I	-0.56	74
		II	-0.18	87
Na ₃ Bi	p	II	-0.18	7.5
	n	I	0.94	10
BiTeCl	p	I	-0.71	4
		II	-0.47	2.5
	n	I	0.72	8
		II	0.29	1.5
YPtBi	n	I	0.44	18
		II	0.05	8
TaAs	n	III	0.085	53

A. Band and Topological Insulators

Strained [37] β -As₂Te₃ has an electronic structure with a vanishing band gap (see Fig. 3a). As a result, it has nonzero DOS throughout the energy window chosen (see Fig. 2a). Furthermore, its DOS is symmetric about the Fermi level. As a result, we find that its power factor is also roughly symmetrical, exhibiting two peaks (type-I and type-II) for the n-type doping and two peaks (type-I and type-II) for the p-type doping (see Fig. 2a). A maximum power factor of $57 \times 10^{14} \mu W cm^{-1} K^{-2} s^{-1}$ is observed for p-type doping at $E_F = -0.44$ eV (see Table II). In contrast, the maximum power factor of *unstrained* β -As₂Te₃ (see Fig. 4b) is relatively weaker ($\sim 40 \times 10^{14} \mu W cm^{-1} K^{-2} s^{-1}$) occurring in the n-type region. The peaks in the p-doped region of unstrained β -As₂Te₃ are about 2.5 times weaker than those of strained β -As₂Te₃, showing the tunability of thermoelectric properties with strain, as is the tunability of electronic topology.

Electronic structure of PbTe at the experimental lattice constant (see Fig. S1) exhibits a zero band gap, which is far from its experimentally observed band gap of 0.3-0.4 eV. DFT calculations are known to generally underestimate electronic band gap (E_g), and this is further complicated here by the fact that gap depends on strain. An E_g is central to the TE properties of a material, we calculate the electronic structure of PbTe at applied isotropic strain $\epsilon_h = 0.02$ and $\epsilon_h = -0.01$ [38] (strain is applied with respect to the experimental lattice constant, a_{exp}). At $\epsilon_h=0.02$, PbTe is a band insulator (lattice constants; a_{BI}) with a band gap of 0.11 eV (see Fig. 4c) and at $\epsilon_h=-0.01$, PbTe is in the TCI phase (lattice constant; a_{TCI}) with $E_g=0.1$ eV (see Fig. 3c). Remarkably, the dependence of power factor on doping concentrations is quite similar at both the lattice constants (see Fig. 2c and Fig. 4d). While P exhibits no peaks for n-type doping (see Fig. 2c and Fig. 4d), we find two peaks when the Fermi level enters the VB. As can be expected for PbTe, the peaks have high power factors with rather similar strengths ($70-90 \times 10^{14} \mu W cm^{-1} K^{-2} s^{-1}$) for both the band and topological insulating phases. We find that only type-II peak occurs around $E_F = -0.18$ eV (see Table II), and therefore this is more relevant to achieving high performance TE experimentally. We also find that this peak is marginally stronger for topological insulating phase ($\sim 77 \times 10^{14} \mu W cm^{-1} K^{-2} s^{-1}$) than for band insulating ($\sim 72 \times 10^{14} \mu W cm^{-1} K^{-2} s^{-1}$), while their band gaps are similar. On applying larger compressive strains ($\epsilon_h = -0.014$), band gap of PbTe widens further to 0.23 eV (see Fig. S2) leading to enhancement in the type-II

peak to $\sim 90 \times 10^{14} \mu W cm^{-1} K^{-2} s^{-1}$ with large Seebeck coefficient, S (see supplementary Fig. S3). This is rather interesting as the band gap of PbTe for $\epsilon_h = -0.014$ is closer to the one observed experimentally, which is more appropriate to enhance ZT of compounds with electronic structure similar to that of SnTe [18, 19].

BiTeCl is a large band gap ($E_g = 0.5$ eV) material (see Fig. 3b). Its conductivity is essentially zero for Fermi energy lying within the band gap (see Fig. 2b). Moreover, its DOS also grows very gradually on entering the VB and CB edges. It exhibits four peaks in its power factor, similar to β -As₂Te₃, with both n-type and p-type doping regions having both type-I and type-II peaks (see Fig. 2b). Among all the peaks, a maximum P (type-I) of $8 \times 10^{14} \mu W cm^{-1} K^{-2} s^{-1}$ appears at $E_F = 0.72$ eV in the n-doped region (see Table-II). Low value of P in BiTeCl practically rules it out from any thermoelectric applications.

B. Topological, Dirac and Weyl Semimetals

Na₃Bi exhibits two types of peaks (type-I and type-II) in its power factor as a function of E_F . A maximum power factor (type-I peak) of $10 \times 10^{14} \mu W cm^{-1} K^{-2} s^{-1}$ occurs at $E_F = 0.94$ eV (see Table II) for the n-doped region, while in the p-doped region it exhibits a type-II peak with a maximum power factor of $7.5 \times 10^{14} \mu W cm^{-1} K^{-2} s^{-1}$ (see Table II). Unlike strained β -As₂Te₃, the variation in its DOS with energy is rather weak, thereby leading to a relatively small S and P .

YPtBi is a zero band gap material and its DOS increases rather sharply at $E_F = 0.44$ eV due to the lowest conduction band which is flat (see Fig. 3d). However, due to its low S and σ , its thermoelectric power is rather small, with both type-I and type-II peaks in the n-doped region (see Fig. 2d). YPtBi belongs to the class of group IIIB-(Ni, Pd, Pt) type half-Heusler (HH) alloys [40], which, based on their n-type power factors, are expected to perform better as a thermoelectric material than the widely studied group IVB-Ni type HHs [45–48]. The maximum power factor (type-I peak) of YPtBi is $18 \times 10^{14} \mu W cm^{-1} K^{-2} s^{-1}$, close to the maximum n-type power factors among HHs (LaPdBi with P of $25 \times 10^{14} \mu W cm^{-1} K^{-2} s^{-1}$) [40]. Unlike other materials studied here, S of YPtBi increases with temperature, which could favor its use in high temperature thermoelectric transport applications.

TaAs has a very small band gap (0.032 eV), and it exhibits only a single type-III peak (maximum power factor of $53 \times 10^{14} \mu W cm^{-1} K^{-2} s^{-1}$) in the power factor. This peak in P

occurs at low concentration of n-type doping around $E_F=0.085$ eV. This single large peak arises from the coincidence of the maxima of S and $[\frac{\partial D(\epsilon)}{\partial \epsilon}]$. Maximum of P of this compound is similar in magnitude to the maximum P of β -As₂Te₃ (i.e. $57 \times 10^{14} \mu W cm^{-1} K^{-2} s^{-1}$). Hence, we predict that TaAs, whose TE properties are yet to be explored experimentally, could be a high performance TE material.

V. DISCUSSION

A. Multiple Band Extrema and Sub-band Structure

Both strongly dispersing and dispersion-less flat electronic bands play different roles in enhancing TE properties [49]. For example flat bands increase DOS and contain high effective mass charge carriers suitable for a large thermopower S (see Eq. [1]), whereas bands with a high curvature on the other hand contain light charge carriers favorable for electronic conductivity (see Eq. [2]). Amongst the compounds considered here, only YPtBi and TaAs contain transition metal (d-type valence electrons) atoms. Except for YPtBi however, bands of all other compounds are rather strongly dispersing (see Fig. 3). Despite this, we find a strong contrast in the TE properties of these compounds. For example, among Na₃Bi and strained [38] β -As₂Te₃ with zero band gaps, Na₃Bi is a poor thermoelectric (see Fig. 2e), while strained β -As₂Te₃ (see Fig. 2a) exhibits a high P for both p and n type doping (see Table II). To understand this, we compare the electronic structure of the two compounds (see Figs. 3a & 3e). We notice that the electronic structure of strained β -As₂Te₃ exhibits numerous extrema (peaks) in its electronic bands close to the Fermi level other than its VBM and CBM (see Fig. 3a). For example, it has valence band extrema (VBE) lying along the path Γ -Z-F- Γ -L paths. These VBE are within 0.3 eV below the Fermi level and enhance the DOS. These VBE also favor electronic conductivity as they contain light hole carriers, thereby enhancing P in both the ways. Undoped Na₃Bi does not exhibit VBE or conduction band extrema (CBE) (see Fig. 3e) around the Fermi level (within ~ 1 eV), and is relatively poorer TE.

Due to rather similar dispersion of electronic bands of most compounds studied here (except YPtBi), we identify the presence of these features of extrema in the electronic structure as the criterion for large power factor in topologically non-trivial materials. This

is manifesting quite clearly in the electronic structure of PbTe and TaAs (see Fig. 3c and 3f) which exhibit significant P for only one type of doping (see Fig. 2c and 2f). This is due to the striking difference in DOS of VB and CB (see Fig. 2f and 2c) of these compounds. Similar to strained β -As₂Te₃ (see Fig. 3a), TaAs exhibits CBE along Σ_1 -Z, Γ -X and VBE along N- Σ_1 -Z, which enhance the DOS. Moreover, closely spaced peaks in the spin-split bands of TaAs along Σ -N- Σ_1 around the Fermi level could be controlled favorably towards band convergence, which can enhance TE performance. Similarly, PbTe exhibits VBE along W- Γ -X which gives rise to a sharp increase in its DOS (see Fig. 2c) of its VB. Power factor of YPtBi also exhibits moderate values only for n-type doping (see Table II), due to large DOS of its CB however arising from a relatively flat d band just above the undoped Fermi level (see Figure 3d). Thus, electronic bands of topologically non-trivial materials are usually strongly dispersing, and large values of P are observable mostly when the band structure has other VBE/CBE (or peaks) lying close (within 0.5 eV) to the VBM/CBM.

B. Tunability with Strain : ETT and Convergence of Bands

The thermoelectric power factors of TIs and TCIs are found to be quite sensitive to strain. Applying large enough compressive strains ($\epsilon_h = -0.014$), thermoelectric power of PbTe increases from 72 \rightarrow (see Fig. 4d) to $90 \times 10^{14} \mu W cm^{-1} K^{-2} s^{-1}$ (see Fig. S3) due to the widening the band gap from 0.11 eV (see Fig. 4c) to 0.23 eV (see Fig. S2). Our estimates of E_g at the experimental lattice constants of PbTe is 0 eV which is far from its experimental value, implying that the actual strains required to obtain larger band gaps in the TCI phase of PbTe might be a bit larger than the one estimated here ($\epsilon_h = -0.014$). However, our results suggest a robust mechanism for enhancement of P in topologically nontrivial materials in general. Due to the phenomenon of band inversion, the CB and VB can be inverted and band gap of bulk TIs and TCIs can be closed and reopened with application of pressure or strain. This provides a unique way of controlling E_g of those materials which is central to their TE properties. E_g of a material undergoing an ETT can be increased upon application of appropriate compressive stresses, *irrespective* of whether they are in their BI or TI phases. Compressive stresses on TE modulators, which are typically flat devices, can be achieved readily by applying a mechanical load, which is much more practical than application of shear or tensile stresses. Small E_g is a primary concern in materials such as SnTe ($E_g =$

0.18 eV at 300 K) which otherwise have suitable electronic structure for TE applications. As PbTe is in the vicinity of an ETT, its E_g can be tuned by applying external stresses. Thus, we argue that TE devices based on small E_g TIs/TCIs can operate more efficiently under mechanical loads.

Change in E_g of β -As₂Te₃ with strain (see Fig. 3a and Fig. 4a) results in considerable changes in its transport properties. While the maximum Seebeck coefficient (S_{max}) in strained β -As₂Te₃ (see Fig. 2a) decreases by 45% compared to S_{max} of unstrained β -As₂Te₃ (see Fig. 4b), its electrical conductivity (σ) increases by a factor of ~ 3 . While P in the n-doped region remain similar, it increases by a factor of ~ 3 for p-type doping on application of uniaxial strain which shifts the maximum of the peaks in P from n-doped to p-doped region. This asymmetric increase in P is attributed to the stronger energy dependence of DOS of the VB of strained β -As₂Te₃. The origin of this enhanced DOS of strained β -As₂Te₃ lies in the convergence of valence bands induced by strain. The VBE like feature along Z-F- Γ paths of ambient β -As₂Te₃ converge into a smaller energy range on application of strain ($\epsilon_{zz} = -0.07$), thereby increasing DOS near the VBM. As discussed above, strained β -As₂Te₃ also exhibits additional VBEs along Γ -Z-F- Γ -L, and exhibits superior thermoelectric properties. Experimentally synthesized β -As₂Te₃ doped with Sn, however, are intrinsically hole doped because of native defects and shows a maximum ZT of 0.65 at 423K [31]. On the other hand, our calculations suggest that the asymmetric increase in P favoring p-type doping on application of uniaxial stress could increase ZT of β -As₂Te₃ significantly.

Our analysis of TE performance of topologically non-trivial bulk phases of the materials does not include the effects of their conducting surface states. Secondly, the stress induced band convergence observed in β -As₂Te₃, may not be unique only to topological insulators. Thus, it would be interesting to identify conditions under which topological non-trivial phase of a material (e.g. a TI) could outperform the corresponding trivial phase (e.g. a BI) of the same compound. Based on our results, we believe that the TE performance of a TI phases is better than its BI phase due to its electronic structure features associated with band inversion (see Fig. 5 for schematic of band edges associated with BI and TI phases). Band inversion in a TI phase lead to extra sharp edges in the DOS of its VB and CB, in addition to the VBM and CBM resulting in a higher DOS of the light carrier bands. This is one of the recipes for attaining a high power factors in bulk TIs.

Thus, not all materials with nontrivial electronic topology exhibit superior thermoelectric

performance. Indeed, a Dirac semi-metal with a vanishing gap may not exhibit high electrical conductivity or Seebeck coefficient. We do demonstrate that a topological insulating state of the *same* compound has better thermoelectric properties than its normal insulating state. Since the nontrivial electronic topology is characterized essentially by a quantized invariant, it is not quite possible to connect such an integer (electronic topology) to thermoelectric properties in simple way. Instead, we connect the two by identifying the mechanisms of high thermoelectric performance in terms of features of electronic structure that are seen in topological materials. Most materials with nontrivial electronic topology exhibit electronic topological transitions (ETT) induced by strain or pressure [14, 51]. A typical ETT between trivial and nontrivial topological insulators involves band inversion or the reversal of the sign of the effective masses. This results in multiple extrema in the valence and conduction bands giving an asymmetry in the nature of valence and conduction bands. Secondly, the sensitivity of electronic structure of these materials to strain (or electron-phonon coupling) is responsible for the tunability of the band extrema and hence the thermoelectric properties through “band convergence” [3].

Amongst the new materials investigated here, the maximum power factor of n-doped TaAs (see Fig. 2f) is similar ($53 \times 10^{14} \mu W cm^{-1} K^{-2} s^{-1}$) to that of good TE materials studied recently like β -As₂Te₃ [31] (which has a maximum power factor of $57 \times 10^{14} \mu W cm^{-1} K^{-2} s^{-1}$, see Table II). The electronic band gap of TaAs can be increased through suitable alloying which may enhance its TE power factor considerably. Furthermore, due to the heavy atomic masses of Ta and As and low frequencies of vibration, a low lattice conductivity is also expected, which would increase the ZT of TaAs. Since the spin orbit coupling is often responsible for nontrivial electronic topology, many of the compounds with nontrivial topology involve heavy elements, and hence have low elastic moduli and thermal conductivity which add to their thermoelectric efficiency.

VI. SUMMARY

Our theoretical analysis of thermoelectric properties of topologically non-trivial materials reveals that (a) topological insulators with small band gaps are excellent TE, while Dirac semimetals may not be quite so, (b) while topological semimetals exhibit relatively poorer TE power, a Weyl semimetal shows good TE power factor. We identify two mechanisms: (i)

band inversion at an electronic topological transition results in many local extrema in the valence and conduction bands, enhancing the density of electronic states and its asymmetry near the Fermi level to give enhanced conductivity and Seebeck coefficient, and (ii) energies of the extrema in VB and CB can be controlled with external strain facilitating *band convergence* [3], which is key to TE properties. Thus, the power factor exhibits multiple peaks (type-I, type-II and type-III) as a function of Fermi energy or doping, which can be tuned with strain. We demonstrated that the band convergence in p-type β -As₂Te₃ with -7% strains enhances its power factor by a factor of 3. Similar effects found in PbTe suggest that TE modulators based on such TIs could operate more efficiently under weak stress. Among the topological and band insulating states of a compound with the same band gap, TE performance of the TI state is superior. Finally, we predict that TaAs, a Weyl semimetal, is a promising TE and should be explored experimentally.

VII. ACKNOWLEDGEMENTS

UVW thanks Department of Science and Technology, Government of India for funding through a TUE-CMS project of Nano Mission and support through a JC Bose National Fellowship.

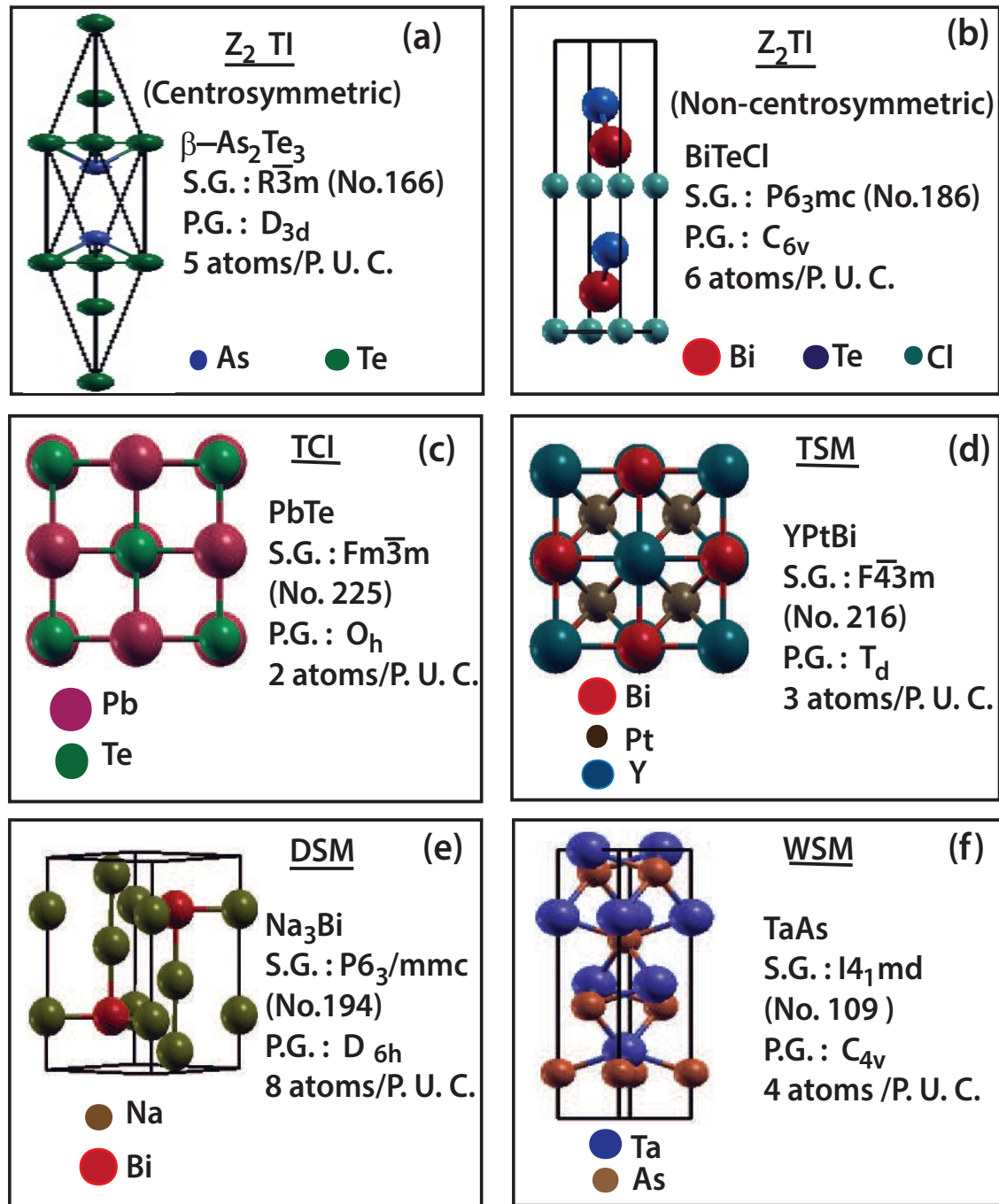


FIG. 1. (Color online)–Crystal structures, space group (S.G.), point group (P.G.) symmetries of the six materials used in this work. The abbreviations TI, TCI, DSM, TSM, and WSM stand for topological insulator, topological crystalline insulator, Dirac semimetal, topological semimetal, and Weyl semimetal respectively. P.U.C stands for primitive unit cell.

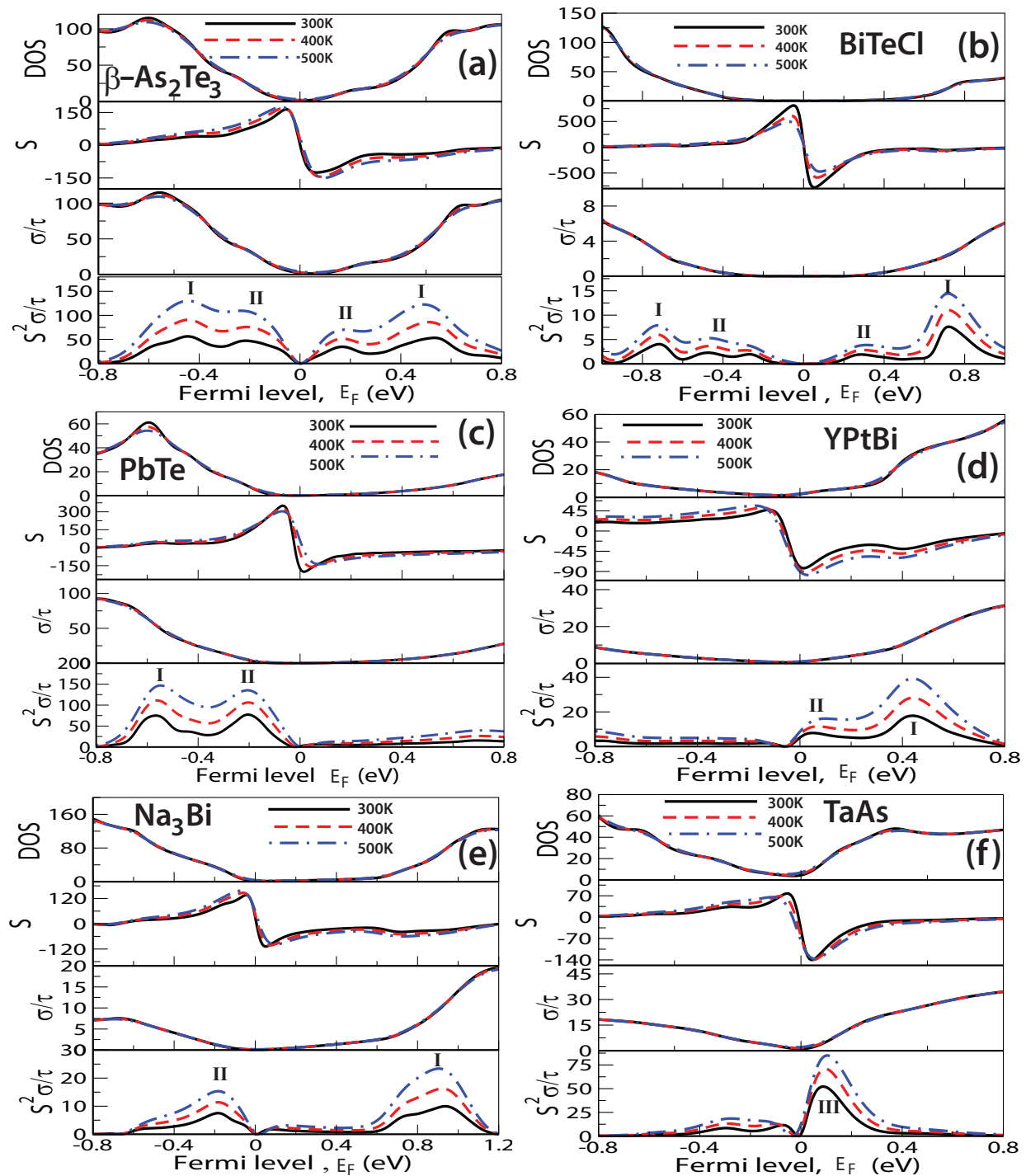


FIG. 2. (Color online)–Dependences of density of state (DOS), electrical conductivity (σ/τ), Seebeck coefficient (S), power factor ($S^2\sigma/\tau$) on Fermi levels at different temperatures. Units for DOS, σ/τ , S , $S^2\sigma/\tau$ are number of states per eV per unit cell, $10^{17} \Omega^{-1} \text{cm}^{-1} \text{s}^{-1}$, $\mu \text{V K}^{-1}$ and $10^{14} \mu \text{W cm}^{-1} \text{K}^{-2} \text{s}^{-1}$ respectively. Type-I, type-II and type-III peaks are marked respectively with I, II and III either just above or below each peak in the power factor vs Fermi energy (E_F) graphs. Results for three different temperatures 300 K, 400 K and 500 K are indicated with black (solid line), blue (dashed line) and red (dash dotted line) colors respectively.

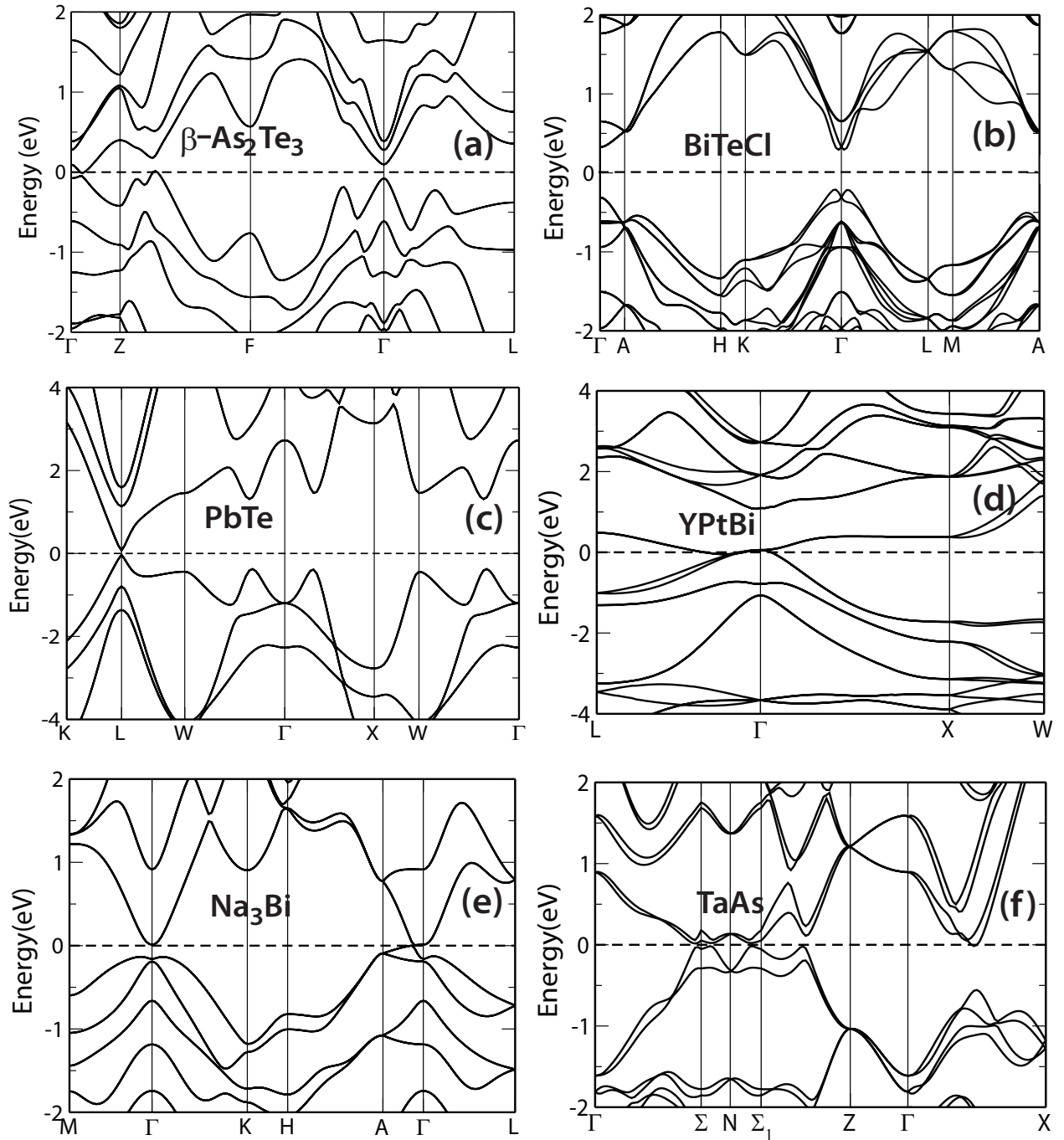


FIG. 3. Electronic structure of the bulk of the six materials under consideration calculated with spin orbit coupling along the high symmetry directions of their Brillouin zones. Electronic structures for all these materials are calculated at their experimental lattice constants except for $\beta\text{-As}_2\text{Te}_3$ and PbTe for which their native states have trivial electronic topology (see Table I).

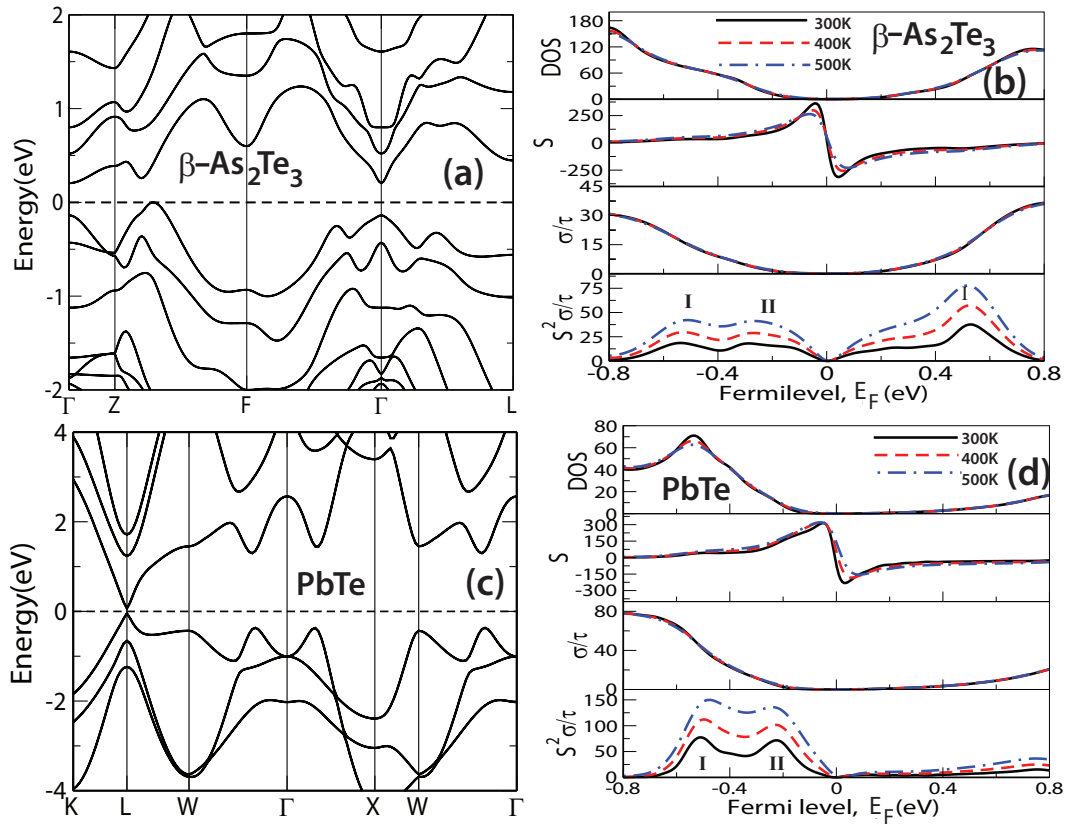


FIG. 4. (Color online)–Electronic structure, density of states (DOS) and transport properties ($S, \sigma/\tau, P$) for unstrained $\beta\text{-As}_2\text{Te}_3$ (a, b) and strained ($\epsilon_h=0.02$, $a_{BI} = 6.567 \text{ \AA}$, $E_g = 0.11 \text{ eV}$) PbTe (c, d). a_{BI} is the lattice constant of the band insulating phase of PbTe. In Fig. 4b and 4d Type-I, type-II and type-III peaks in the power factors (P) are marked respectively with Roman numerals I, II, and III. Results for three different temperatures 300 K, 400 K and 500 K are indicated with black (solid line), blue (dashed line) and red (dash dotted line) colors respectively in Fig. 4b and Fig. 4d.

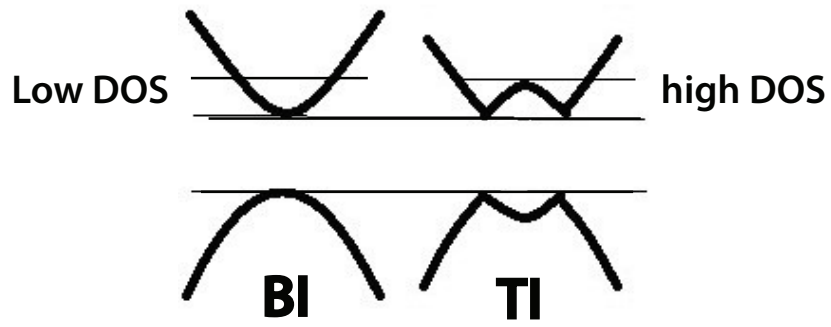


FIG. 5. Schematic picture of band inversion between the valence band maximum (VBM) and conduction band minimum (CBM). Band insulator and topological insulator are denoted with BI and TI respectively. Due to band inversion, in TI phase, the density of states (DOS) near the Fermi level is higher than that of band insulator.

-
- [1] G. J. Snyder and E. S. Toberer, *Nature Mat.*, 2008, **7**, 105-114.
- [2] D. Kraemer et al., *Nature Mat.*, 2011, **10**, 532-538.
- [3] Y. Pei, X. Shi, A. LaLonde, H. Wang, L. Chen and G. J. Snyder *Nature*, 2011, **473**, 66-69.
- [4] G. S. Nolas, J. Poon and M. Kanatzidis, *MRS Bull.*, 2008 **31**, 199-205.
- [5] T. M. Tritt and M. A. Subramanian, *MRS Bull.*, 2006. **31**, 188-198.
- [6] H. Böttner, G. Chen and R. Venkatasubramanian, *MRS Bull.*, 2006 **31**, 211-217.
- [7] J. Yang and T. Caillat, *MRS Bull.*, 2008, **31**, 224-229.
- [8] R. Franz, G. Wiedemann, *Ann. der Physik*, 1853, **165**, 497-531.
- [9] M. Cutler and N. F. Mott, *Phys. Rev.*, 1969, **181**, 1336-1340.
- [10] J. P. Heremans et al., *Science*, 2008, **321**, 554-557.
- [11] G. D. Mahan and J. O. Sofo, *Proc. Natl. Acad. Sci.*, 1996, **93**, 7436-7439.
- [12] Y. L. Chen J. G. Analytis, J.-H. Chu, Z. K. Liu, S.-K. Mo, X. L. Qi, H. J. Zhang, D. H. Lu, X. Dai, Z. Fang, S. C. Zhang, I. R. Fisher, Z. Hussain, Z.-X. Shen, *Science*, 2009, **325**, 178-181.
- [13] H. Zhan, C.-X. Liu, X.-L. Qi, X. Dai, Z. Fang and S.-C. Zhang, *Nature Phys.*, 2009, **5**, 438-442.
- [14] P. Barone, T. Rauch, D. D. Sante, J. Henk, I. Mertig, and S. Picozzi, *Phys. Rev. B*, 2013, **88**, 045207.
- [15] L. Muchler, F. Casper, B. Yan, S. Chadov, C. Felser, *Phys. Status Solidi RRL*, 2013, **7**, 91-100.
- [16] X. Chen, D. Parker, and D. J. Singh, *Sci. Rep.* **3**, 3168 (2013).
- [17] H. Shi, D. Parker, M.-H Du, and D. J. Singh, *Phys. Rev. Appl.*, 2015, **3**, 014004.
- [18] A. Banik, U. S. Shenoy, S. Anand, U. V. Waghmare, and K. Biswas, *Chem. Mater.*, 2015, **27(2)**, 581-587.
- [19] G. Tan, F. Shi, J. W. Doak, H. Sun, L.-D. Zhao, P. Wang, C. Uher, C. Wolverton, V. P. Dravid and M. G. Kanatzidis, *J. Am. Chem. Soc.*, 2014, **136(19)**, 7006-7017.
- [20] Y. Xu, Z. Gan, and S.-C. Zhang, *Phys. Rev. Lett.*, 2014, **112**, 226801(1)-226801(5).
- [21] Z. K. Liu, J. Jiang, B. Zhou, Z. J. Wang, Y. Zhang, H. M. Weng, D. Prabhakaran, S-K. Mo, H. Peng, P. Dudin, T. Kim, M. Hoesch, Z. Fang, X. Dai, Z. X. Shen, D. L. Feng, Z. Hussain and Y. L. Chen, *Nature Mat.*, 2014, **13**, 677-681.
- [22] Z. K. Liu, B. Zhou, Y. Zhang, Z. J. Wang, H. M. Weng, D. Prabhakaran, S.-K. Mo, Z. X. Shen, Z. Fang, X. Dai, Z. Hussain, Y. L. Chen, *Science*, 2014, **343**, 864-867.

- [23] S. M. Huang et al., arXiv 1501.00755 (2015).
- [24] L. Fu, *Phys. Rev. Lett.*, 2011, **106**, 106802(1)-106802(4).
- [25] T. H. Hsieh, H. Lin, J. Liu, W. Duan, A. Bansil and L. Fu, *Nature Comm.*, 2012, **3**, 982, 1-6.
- [26] M. König et al., *Science*, 2007, **318**, 766-770.
- [27] Q. Gibson, L. M. Schoop, L. Muechler, L. S. Xie, M. Hirschberger, N. P. Ong, R. Car, and R. J. Cava, *arXiv.1411.0005v1*, 2014, 1-26.
- [28] K. Pal and U. V. Waghmare, *App. Phys. Lett.*, 2014, **105**, 062105(1)-062105(5).
- [29] Y. L. Chen, M. Kanou, Z. K. Liu, H. J. Zhang, J. A. Sobota, D. Leuenberger, S. K. Mo, B. Zhou, S-L. Yang, P. S. Kirchmann, D. H. Lu, R. G. Moore, Z. Hussain, Z. X. Shen, X. L. Qi, and T. Sasagawa, *Nature Phys.*, 2013, **9**, 704-708.
- [30] W. Al-Sawai, H. Lin, R. S. Markiewicz, L. A. Wray, Y. Xia, S.-Y. Xu, M. Z. Hasan, and A. Bansil, *Phys. Rev. B*, 2010, **82**, 125208(1)-125208(5).
- [31] J.-P. Vaney, J. Carreaud, G. Delaizir, A. Pradel, A. Piarristeguy, C. Morin, E. Alleno, J. Monnier, A. P. Gonçalves, C. Candolfi, A. Dauscher, and B. Lenoir, *Adv. Electron. Mater.*, 2015, **1**, 1400008, 1-5.
- [32] P. Blaha, K. Schwarz, G. K. H. Madsen, D. Kvasnicka and J. Luitz, WIEN2k, An Augmented Plane Wave Local Orbitals Program for Calculating Crystal Properties (K 2001. ISBN 3-9501031-1-2).
- [33] J. P. Perdew, K. Burke, M. Ernzerhof, *Phys. Rev. Lett.*, 1996, **77**, 3865.
- [34] X. Hua, X. Chen, W. A. Goddard III, *Phys. Rev. B*, 1997, **55**, 16103.
- [35] A. H. MacDonald, W. E. Pickett, and D. D. Koelling, *J. Phys. C*, 1980, **13**, 2675.
- [36] P. Novak, F. Boucher, P. Gressier, P. Blaha, and K. Schwarz, *Phys. Rev. B*, 2001, **63**, 235114.
- [37] β -As₂Te₃ is a band insulator but it undergoes electronic topological transition at $\epsilon_{zz}=-0.05$. So here, we are calculating the transport properties at $\epsilon_{zz}=-0.07$ where β -As₂Te₃ is in the topological insulating state.
- [38] PbTe is a band insulator at ambient pressure. According to our first-principles calculation, at the experimental lattice constant ($a_{exp}=6.4384 \text{ \AA}$ [50]), PbTe exhibits zero band gap (see Fig. S1 in the Supplementary material section). To compare the thermoelectric performance of the band insulating and topological crystalline insulating phases, we increased the lattice constant isotropically by 2% and decreased it by 1% respectively with respect to a_{exp} . With these values of strains, both the TI and BI phases have comparable band gaps of 0.1 and 0.11

eV respectively We also calculate the electronic structure and transport properties of PbTe with -1.4% hydrostatic strain, where it has a band gap of 0.23 eV. The results corresponding to -1.4% isotropic strain are given Fig. S3 of the Supplementary material.

- [39] G. K. H. Madsen and D. J. Singh, *Comp. Phys. Comm.*, 2006, **175**, 67.
- [40] J. Yang, H. Li, T. Wu, W. Zhang, L. Chen and J. Yang, *Adv. Fun. Mater.*, 2008, **18**, 2880-2888.
- [41] T. J. Scheidemantel, C. A.-Draxl, T. Thonhauser, J. V. Badding, and J. O. Sofo, *Phys. Rev. B*, 2003, **68**, 125210.
- [42] G. K. H. Madsen, *J. Am. Chem. Soc.*, 2006, **128**, 12140-12146.
- [43] L. Chaput, P. Pécheur, J. Tobola, and H. Scherrer, *Phys. Rev. B*, 2005, **72**, 085126.
- [44] X. Gao, K. Uehara, D. D. Klug, S. Patchkovskii, J. S. Tse, and T. M. Tritt, *Phys. Rev. B*, 2005, **72**, 125202.
- [45] C. Uher, J. Yang, S. Hu, D. T. Morelli, and G. P. Meisner, *Phys. Rev. B*, 1999, **59**, 8615.
- [46] Q. Shen, L. Chen, T. Goto, T. Hirai, J. Yang, G. P. Meisner and C. Uher, *Appl. Phys. Lett.*, 2001, **79**, 4165-4167.
- [47] S. Bhattacharya, T. M Tritt, Y. Xia, V. Ponnambalam, S. J. Poon, N. Thadhani, *Appl. Phys. Lett.*, 2002, **81**, 43-45.
- [48] S. Sakurada and N. Shutoh, *Appl. Phys. Lett.*, 2005, **86**, 082105.
- [49] K. Kuroki and R. Arita, *J. Phys. Soc. Jpn.*, 2007, **76**, 083707.
- [50] Y. Noda, K. Masumoto, S. Ohba, Y. Saito, K. Toriumi, Y. Iwata, I. Shibuya, *Acta Cryst., Section C: Cryst. Struct. Comm.*, 1987, **43**, 1443.
- [51] A. Bera, K. Pal, D. V. S. Muthu, S. Sen, P. Guptasarma, U. V. Waghmare, and A. K. Sood, *Phys. Rev. Lett.*, 2013, **110**, 107401.

TOC:

Small band gap topological insulators and Weyl semimetals show excellent TE properties. We identify two mechanisms (a) asymmetry in the electronic density of states caused by band inversion at an electronic topological transition and (ii) band convergence as the key to good TE behavior in these materials.

